RESEARCH PAPER

Formulations of a hydromechanical interface element

Zhong-Zhi Fu · Si-Hong Liu

Abstract A hydromechanical interface element is proposed for the consideration of the hydraulic-mechanical coupling effect along the interface. The fully coupled governing equations and the relevant finite element formulations are derived in detail for the interface element. All the involved matrices are of the same form as those of a solid element, which makes the incorporation of the model into a finite element program straightforward. Three examples are then numerically simulated using the interface element. Reasonable results confirm the correctness of the proposed model and motivate its application in hydromechanical contact problems in the future.

Keywords Hydromechanical interface element · Coupling effect · Finite element · Contact problem

1 Introduction

It is well recognized that the existence of discontinuities in geotechnical engineering may significantly influences the mechanical and hydraulic responses of surrounding structures and foundations [1–4], such as the stress distribution in a jointed arch dam during an earthquake and the seepage behavior of the dam foundation where a concrete cutoff wall has been constructed. Generally, it is rather difficult to take all the discontinuities into account when they are densely and randomly distributed within a host medium like fractured rocks, and a reasonable approach to solve this kind of problem is to take the fractured medium as a porous one so that an exact identification of the discontinuities is avoided [5, 6]. Special attention, however, should be paid to the heterogeneity and anisotropy effect of the medium during the multi-physical processes [5, 6]. On the other hand, if the discontinuities are countable and easily located, it is possible to take them into consideration during physical processes in a much more direct and precise way. This is the so-called interface problem, where thermal, hydraulic and mechanical processes may be involved. In the present study, the thermal process is neglected and only the mechanical and hydraulic processes are considered for an interface.

Generally, contact mechanics [7–11] focuses on the mechanical response along the probable contact surfaces while fracture hydraulics [12–15] takes the seepage behavior within the discontinuities as the main concern. However, in many geotechnical engineering, the mechanical and hydraulic behaviors within the interface appear combined and influence each other, leading to the so-called hydromechanical coupling effect [4, 13]. Taking the mechanical and seepage behaviors near the cutoff wall as an example, the opening and closure of the gap between the riverbed and the cutoff wall, governed mainly by external loads and the mechanical response of the materials, can evidently change the seepage path around the cutoff wall; on the other hand, the seepage behavior along the interface controls the accumulation and dissipation of the excessive pore water pressure near the cutoff wall and subsequently influences the contact status along the interface.

To simulate the hydromechanical coupling effect along the interface in engineering, it is reasonable to combine a contact algorithm with a fracture seepage model and construct a mathematical model for the interface. Furthermore, the model should be simple so that its implementation in numerical tools is convenient. It was proved that a mechanical contact problem is equivalent to an optimization problem subjected to the kinematical restraint, i.e. the non-penetration condition [7–10]. The Lagrange multiplier

Z.-Z. Fu (✉) · S.-H. Liu
College of Water Conservancy and Hydropower Engineering,
Hohai University, 210098 Nanjing, China
Email: fu_zhongzhi@yahoo.com

method (LMM) [7] is the fundamental approach for this kind of problem in which the Kuhn–Tucker complementary condition is directly introduced to the potential function of the system, translating the constrained optimization problem into an unconstrained one. Despite the precise satisfaction of the constraint in LMM, the contact forces should also be taken as basic variables as well as the nodal displacements, this makes the implementation of LMM in a standard finite element program inconvenient. Another well known approach for contact problems is the so-called penalty method (PM) [7, 16], in which a small amount of penetration between the neighboring surfaces is allowed and realized by defining a large anti-penetration stiffness, for example the interface elements proposed by Goodman et al. [1] and Simons et al. [16]. Because no additional variables, except the nodal displacements, are introduced in the governing equation, PM can be easily incorporated into an existing finite element program. This probably is the main reason that PM is so widely used in geotechnical applications despite the possibility of an ill-conditioned governing equation [16, 17].

For the simulation of the hydraulic behavior within the interface, special elements with zero-thickness are also used, which can be generally classified into two types depending on the consideration or neglect of the transversal conductivity. When the transversal conductivity is neglected, the physical domain can be discretized without interface elements and the longitudinal flow is modeled by adding "pipe" elements to the edges along the interface [18]. This is similar to the use of truss elements in simulating the anchor bolts in the reinforcement of rock mass. Recently, another kind of interface element was proposed by Segura [12], in which the transversal flow, as well as, the longitudinal flow is included. In this model the transversal flow within the interface is assumed to be governed by the difference of the total hydraulic head at both sides of the interface, and the longitudinal flow velocity is proportional to the gradient of the total hydraulic head. One advantage of Segura's model is the feasibility of using the same mesh for mechanical and seepage analysis or even for fully coupled problems if relevant formulations are established.

Based on the above recapitulation, it seems more convenient to establish a hydromechanical interface element for the analysis of coupled contact problems. This is because we really need an element to consider the mass conservation of the water within the interface when it is open, although the mechanical status of the element is inactive in this case. On the other hand, the mechanical status of the interface element should be activated once the penetration takes place. In this case, the hydraulic status of the interface element may be deactivated. In this paper, we propose a hydromechanical interface element for the simulation of the discontinuities widely presented in geotechnical engineering. The equilibrium equation of the interface element and the mass conservation equation of the water within the interface are then formulated, yielding the finite element formulations of the inter-

face element. The proposed model and derived formulations are finally verified by three examples.

2 Physical background of the interface element

As mentioned already, the penalty method can not prevent surface penetration during loading, which is often regarded as a major insufficiency of those interface elements, i.e. the non-penetration condition can not be satisfied rigorously regardless of the arithmetic error of computers. However, if we pay closer attention to the contact surfaces, we can find that an apparent closed interface (Fig. 1a) does not necessarily indicate that the real boundaries of the related blocks contact seamlessly, which can be attributed to the existence of the micro-asperities built on the surfaces (Fig. 1b). Assume that the contact fronts of two contacting blocks are initially superposed as shown in Fig. 1b, both the separation of the contact fronts and the penetration of the asperities of one block through the contact front of another block can be caused by the external loads. The former may be observed as a separation of two blocks (Fig. 1c) while the latter generally can not be observed with the naked eye (Fig. 1d). This argument seems to confirm the validity of the penetration of surfaces.
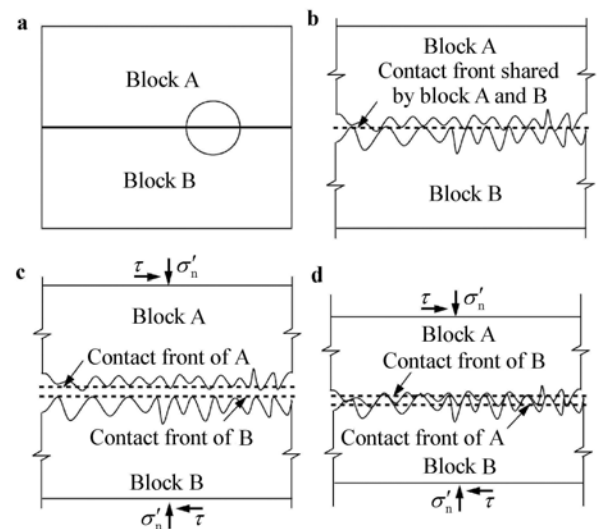
Fig. 1 Micro-inspection of the contact surfaces. **a** Apparent contact status; **b** Microscopic surface geometry; **c** Separation of two blocks; **d** Penetration

A closer inspection of the overlapped zone in Fig. 1d indicates that the interlocked asperities from interfacing surfaces really constitute, to some extent, a new kind of porous medium with different mechanical and hydraulic behaviors from those of its father and mother blocks. Since the thickness of the overlapped zone is very small, the mechanical behavior is usually described using the normal stress and penetration or the shear stress and sliding. For example, the

thickness of the overlapped zone, interpreted as the penetration here, is assumed to be exponentially dependent on the effective normal stress in this study, i.e.

$$\delta_n = \delta_{no} - \delta_{no} \exp\left[-\left(\frac{\sigma'_n}{h_s}\right)^n\right], \tag{1}$$

where δ_n is the current penetration under the normal effective stress σ'_n; δ_{no} is the maximal possible penetration which can be achieved only if the normal stress σ'_n approaches infinity; h_s is a parameter with a dimension of stress and n is a dimensionless constant. It can be concluded that the maximal possible penetration δ_{no} is an overall evaluation of the distribution and geometry of the micro-asperities and the parameter h_s is an overall evaluation of their hardness.

Differentiating Eq. (1) with respect to time and simple mathematical operations leads to the anti-penetration stiffness

$$K_n = \frac{\dot{\sigma}'_n}{\dot{\delta}_n} = \frac{(\sigma'_n/h_s)^{1-n}}{n} \frac{h_s}{\delta_{no} - \delta_n}, \tag{2}$$

in which a superposed dot over a quantity denotes its time derivative. The anti-penetration stiffness is inversely proportional to the unachieved penetration $\delta_{no} - \delta_n$ and tends to be infinite when the penetration approaches the maximal limit, and therefore prevents further penetration.

It is reasonable to postulate that the interlocking of micro-asperities is increasingly pronounced when the penetration increases, therefore the initial anti-sliding stiffness can be assumed to be proportional to the anti-penetration stiffness. However with the increase of shear stress, abrasion of the asperities and shear dilatancy may occur, both of which result in a weaker interlocking effect and subsequently lead to a lower anti-sliding stiffness. In addition, when the shear stress increases to a limit value, which is generally assumed to be proportional to the normal stress according to the Coulomb friction law, the anti-sliding stiffness vanishes absolutely and the interfacing surfaces will slide relatively until a new balanced condition is achieved. Taking these features into consideration, we suggest the following anti-sliding stiffness in this study

$$K_t = \Lambda \cdot K_n \cdot \left[1 - \left(\frac{\tau}{\mu \cdot \sigma'_n}\right)^2\right]^m, \tag{3}$$

where Λ is the proportionality and μ is the friction coefficient; m is a dimensionless constant. Equation (3) is suitable for the description of the shear behavior under monotonic shearing, i.e., $\tau \cdot \dot{\tau} > 0$. In the case where $\tau \cdot \dot{\tau} \leq 0$, the anti-sliding stiffness is assumed to be a constant and equal to the initial value, i.e.

$$K_t = \Lambda \cdot K_n. \tag{4}$$

Figure 2 shows a typical relation predicted by Eqs. (3) and (4). The accumulation of relative sliding can be well reproduced by defining two representations for the anti-sliding stiffness under different conditions. In particular, if the proportionality Λ is high enough, the classical rigid-plastic slip model can be retrieved.
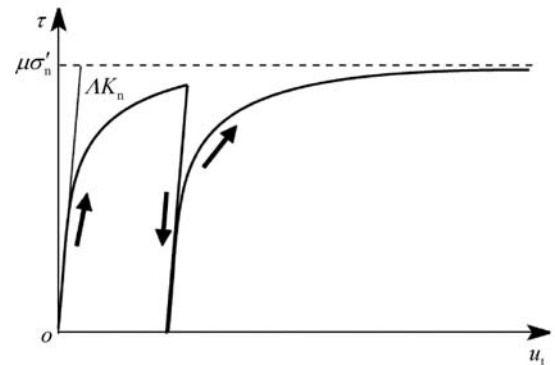
Fig. 2 Shear behavior predicted by Eqs. (3) and (4)

Once the anti-penetration and the anti-sliding stiffness of the interface elements are evaluated, the stiffness matrices of these elements can be calculated and assembled to the global stiffness matrix. Solving the governing equation gives the incremental displacement along the two interfacing surfaces, based on which the contact status can be updated and the cycle of calculation continues. It is not difficult to find that the introduction of interface elements translates a geometrical nonlinear problem to a material nonlinear one, leading to a simpler problem to be solved. In this sense, an approximate satisfaction of the non-penetration condition is enough and most of the parameters involved in the model may not need exact evaluation. However, it is argued that the explicit definition of the maximal possible penetration and the use of asperity hardness as a main physically meaningful parameter enables the modeler to avoid an uncontrollable penetration and an arbitrary definition of the anti-penetration stiffness.

As mentioned previously, the asperities within the overlapped zones constitute a porous medium, which is of course permeable for water. However, the thickness of the effective conducting channel decreases with the penetration as shown in Fig. 3. Besides, further penetration will also result in a lower "porosity" within the overlapped zones and therefore lead to a lower longitudinal permeability coefficient. This concept and the idealized conductive model illustrated in Fig. 3 lead to the assumption that the effective thickness of the conducting channel δ'_n equals the unachieved penetration $\delta_{no} - \delta_n$, on which the longitudinal permeability coefficient is dependent according to the well known cubic law in rock engineering [3, 4], i.e.

$$k_t = \frac{g \cdot \delta'^2_n}{12\nu}. \tag{5}$$

Herein, g denotes the gravity acceleration and ν is the fluid viscosity. For water at 20°C, $\nu \approx 1.01 \, \text{mm}^2/\text{s}$ [3]. Equation (5) is also suitable for the case where the interfacing surfaces are out of contact, and where the "penetration" δ_n should be interpreted as the interfacial gap. It is necessary to

point out that Eq. (5) is based on the assumption that the interfacing surfaces of the parallel plates forming the conducting channel are smooth [14] and the use of Eq. (5) for the penetration condition is not so rigorous. However, a unified representation for the longitudinal permeability coefficient under both the penetrating status and the separating status makes the transition between two statuses continuous, which is very useful for the repression of possible numerical oscillation.
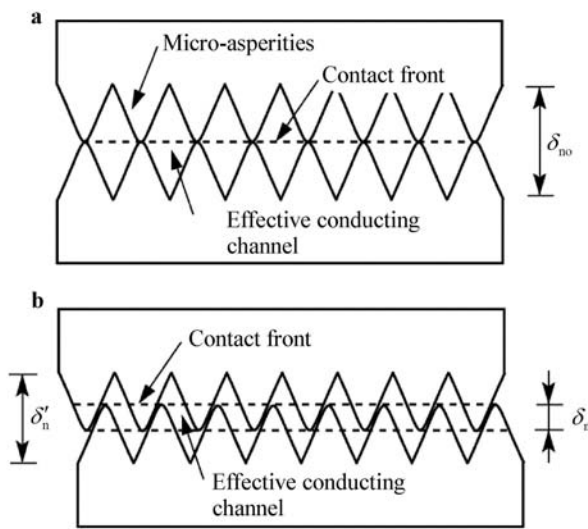
Fig. 3 Idealization of the conductive model. **a** Initial status (no penetration); **b** Penetrating status

In the following part, we always presume that the conducting channels are fully filled with water, i.e. the overlapped porous medium is fully saturated. In this condition, the fluid pressure at a point on one surface can be assumed to be identical to that at the counterpart point on the opposite surface. This restraint can be realized directly by prescribing equivalent degrees of freedom for fluid pressure to those contact node pairs or realized indirectly by modifying the assembled governing equation according to the relevant restraint equations before solving the global equation [12].

3 Finite element formulations of the hydromechanical interface element

To derive the finite element formulations of the hydromechanical interface element, the following naming and translating rules are first introduced: vectors and tensors in the global coordinates (X, Y) are denoted by uppercase letters while the lowercase letters denote the corresponding variables in the local coordinates (x, y) established in the tangential and normal directions of the master surface (Fig. 4a). For example, vector U and vector u denotes the displacement in the global and local coordinates, respectively. They can be

translated mutually using the orthogonal rotating matrix R, i.e.

$$u = R \cdot U, \quad U = R^{\mathrm{T}} \cdot u. \tag{6}$$
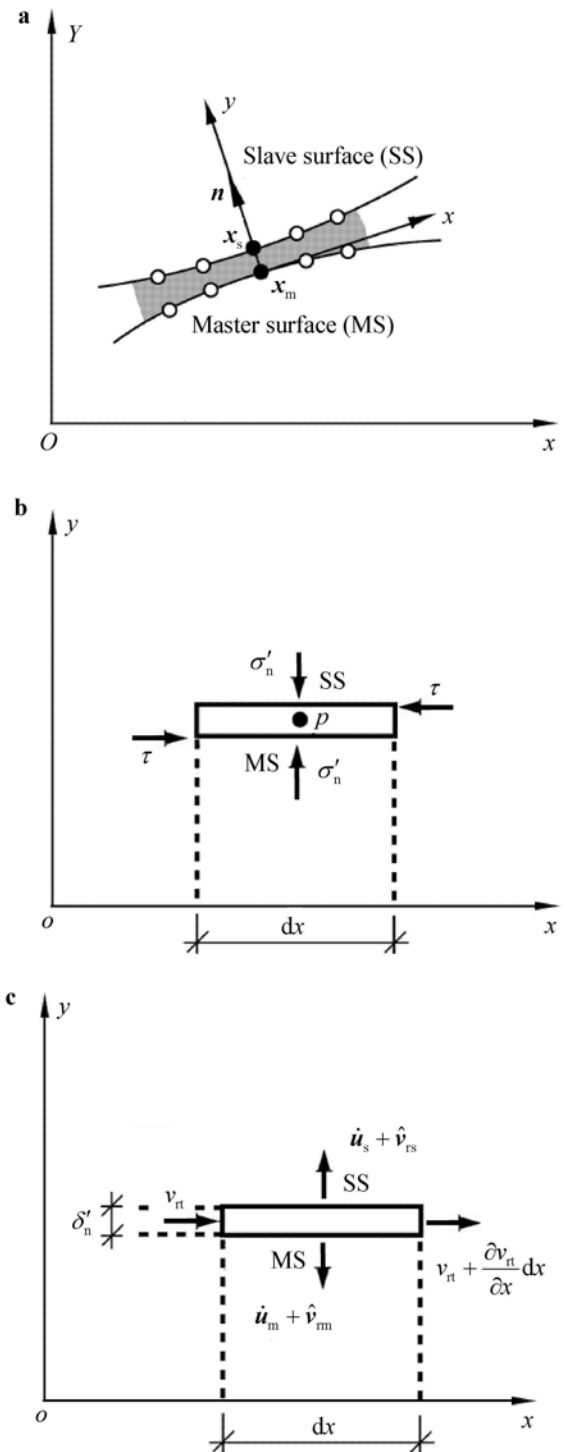
Fig. 4 Mechanical and hydraulic analysis of a coupled interface element. **a** Coupled contact problem; **b** Mechanical analysis; **c** Hydraulic analysis

For small deformation problems, Eq. (6) can also be written in an incremental form, e.g. the incremental force vectors can be translated by the following equations

$$\Delta f = R \cdot \Delta F, \quad \Delta F = R^{\mathrm{T}} \cdot \Delta f. \tag{7}$$

After discretization of the contact surfaces, the relative displacement and the pore pressure at a given point along an interface element can be expressed using the interpolation functions

$$u^{\mathrm{r}} = u_{\mathrm{m}} - u_{\mathrm{s}} = [N_{\mathrm{m}} \quad -N_{\mathrm{s}}] \begin{bmatrix} u_{\mathrm{me}} \\ u_{\mathrm{se}} \end{bmatrix} = B u_{\mathrm{e}}, \tag{8}$$

and

$$p = \frac{1}{2}(p_{\mathrm{m}} + p_{\mathrm{s}}) = \frac{1}{2}[N'_{\mathrm{m}} \quad N'_{\mathrm{s}}] \begin{bmatrix} p_{\mathrm{me}} \\ p_{\mathrm{se}} \end{bmatrix} = N' p_{\mathrm{e}}. \tag{9}$$

Herein, the subscripts "m" and "s" denote master and slave surfaces, respectively; the subscript "e" indicates that the variables are associated with the nodes of an interface element; the superscript "r" in Eq. (8) signifies that the displacement is a relative one defined as the displacement of the master surface minus that of the slave surface. It is also necessary to point out that the interpolation function for pore pressure in Eq. (9) and the assumption of identical pore pressure at the contact node pairs ensures a uniformly distributed fluid pressure in the normal direction of the interface element.

3.1 Equilibrium equation of the interface element

The equilibrium equation of the interface element can be established with the aid of the well known virtual work principle [1]. However, a direct consideration of the equilibrium condition for the interface element leads to the same governing equation.

Assume that a nodal force increment $\Delta F_{\mathrm{e}} = (\Delta F_{\mathrm{me}} \quad \Delta F_{\mathrm{se}})^{\mathrm{T}}$ is exerted to an interface element in equilibrium, leading to an incremental shear and normal stress $\Delta \sigma' = [\Delta \tau \quad \Delta \sigma'_{\mathrm{n}}]$ and an incremental fluid pressure Δp. The incremental effective stress $\Delta \sigma'$ and fluid pressure Δp should exactly balance the external force increment, i.e.

$$\int_{L} B^{\mathrm{T}} R^{\mathrm{T}} (\Delta \sigma' + \Delta p m) \mathrm{d}x = \Delta F_{\mathrm{e}}. \tag{10}$$

Herein, the vector $m = [0 \quad 1]^{\mathrm{T}}$ is introduced for the representation of Terzaghi's effective stress principle and the integration is carried out along the interface. The incremental effective stress in Eq. (10) can be further expressed by the nodal displacement increments via the following constitutive equation

$$\Delta \sigma' = D \Delta u^{\mathrm{r}}, \tag{11}$$

in which $D = \mathrm{diag}[K_{\mathrm{t}} \quad K_{\mathrm{n}}]$. Substituting Eq. (11) into Eq. (10) and recalling the interpolation equations (8) and (9) yields the discretized equilibrium equation of the interface

element, i.e.

$$\left(\int_{L} B'^{\mathrm{T}} D B' \mathrm{d}x \right) \cdot \Delta U_{\mathrm{e}} + \left(\int_{L} B'^{\mathrm{T}} m N' \mathrm{d}x \right) \cdot \Delta p_{\mathrm{e}} = \Delta F_{\mathrm{e}}, \tag{12}$$

where $B' = RB$. Comparing Eq. (12) with the equilibrium equation of a solid element [19], one can find that Eq. (12) has exactly the same form as that of a solid element, both of which give the elementary stiffness and coupling matrices as follows

$$K = \int_{L} B'^{\mathrm{T}} D B' \mathrm{d}x, \quad C = \int_{L} B'^{\mathrm{T}} m N' \mathrm{d}x. \tag{13}$$

It is important to note that the fundamental effective stress principle by Terzaghi will not be suitable for the penetration analysis when Biot's coefficient α is not close to unity [4, 19], i.e. $\Delta \sigma = \Delta \sigma' + \alpha \Delta p m$. However, as a first approximation, Terzaghi's simple effective stress principle serves as a reasonable start point. Moreover, the use of Terzaghi's effective stress principle makes Eq. (12) still sound when the interfacing surfaces are out of contact. Otherwise, Biot's coefficient must be set to unity when the interfacial gap is not closed and the evolution of it must be specified during penetrating, which obviously complicates the problem.

3.2 Mass conservation equation of the water within the interface element

Since the effective conducting channel is assumed to be fully saturated with water, the following local mass conservation equation can be obtained

$$\nabla \cdot v + \frac{\dot{p}}{K_{\mathrm{w}}} = 0, \tag{14}$$

in which v denotes the velocity of water and K_{w} is its bulk modulus. The weak form of Eq. (14) can be established by introducing an arbitrary test function w and integrating Eq. (14) within the effective conducting channel, i.e.

$$\int_{V} w \left(\nabla \cdot v + \frac{\dot{p}}{K_{\mathrm{w}}} \right) \mathrm{d}V = 0. \tag{15}$$

In the following mathematical operations, we assume that the smooth requirement of the test function w can always be satisfied automatically. Using Gaussian integration theorem [19], Eq. (15) can be rewritten as follows

$$\int_{S} w n \cdot v \mathrm{d}S - \int_{V} (w \nabla) \cdot v \mathrm{d}V + \int_{V} w \frac{\dot{p}}{K_{\mathrm{w}}} \mathrm{d}V = 0. \tag{16}$$

Herein, n is the outer normal to the boundary of the interface element. It is important to note that the fluid velocity on the boundary of the conducting channel is composed of the solid velocity $\dot{u}$ and the relative velocity v_{r} while the fluid velocity within the conducting channel is not associated with the velocity of the solid boundary (Fig. 4c), i.e.

$$v = \begin{cases} \dot{u} + \hat{v}_{\mathrm{r}}, & \text{on } S, \\ v_{\mathrm{r}}, & \text{in } V. \end{cases} \tag{17}$$

The coupling effect takes place along the solid-fluid interface and results in the following form of Eq. (16)

$$\int_S w\mathbf{n} \cdot \dot{\mathbf{u}}\,\mathrm{d}S + \int_S w\mathbf{n} \cdot \hat{\mathbf{v}}_r\,\mathrm{d}S$$
$$- \int_V (w\nabla) \cdot \mathbf{v}_r\,\mathrm{d}V + \int_V w\frac{\dot{p}}{K_w}\,\mathrm{d}V = 0. \qquad (18)$$

If we use the same interpolation equation for the test function w as that for the pore pressure p, i.e. $w = \mathbf{N}'\mathbf{w}_e$; $\partial w/\partial y = 0$, then the third term in Eq. (18) can be rewritten as follows

$$\int_V (w\nabla) \cdot \mathbf{v}_r\,\mathrm{d}V = \int_V \frac{\partial w}{\partial x}v_{rt} + \frac{\partial w}{\partial y}v_{rn}\,\mathrm{d}V$$
$$= \int_V \frac{\partial w}{\partial x}v_{rt}\,\mathrm{d}V, \qquad (19)$$

where the fluid velocity in the normal direction v_{rn} disappears automatically while the velocity in the tangential direction v_{rt} remains and can be calculated using Darcy's law [3], i.e.

$$v_{rt} = \frac{k_t}{\rho_w g}\left(-\frac{\partial p}{\partial x} + \rho_w g_t\right) = k'_t\left(-\frac{\partial p}{\partial x} + \rho_w g_t\right). \qquad (20)$$

Herein, ρ_w and g_t denote the density of water and the tangential component of the gravity acceleration along the interface. Based on Eqs. (19) and (20), Eq. (18) can now be expressed in a matrix form

$$-\mathbf{w}_e^T\left(\int_L \mathbf{N}'^T\mathbf{m}^T\mathbf{B}'\mathrm{d}x\right) \cdot \dot{\mathbf{U}}_e + \mathbf{w}_e^T\left(\int_L \mathbf{N}'^T\frac{\delta'_n}{K_w}\mathbf{N}'\mathrm{d}x\right) \cdot \dot{\mathbf{p}}_e$$
$$+\mathbf{w}_e^T\left(\int_L \bar{\mathbf{B}}^T k'_t\delta'_n\bar{\mathbf{B}}\mathrm{d}x\right) \cdot \mathbf{p}_e - \left(\mathbf{w}_e^T\int_L \bar{\mathbf{B}}^T k'_t\delta'_n\rho_w g_t\right)\mathrm{d}x$$
$$+\left(\mathbf{w}_e^T\int_S \mathbf{N}'^T\mathbf{n} \cdot \hat{\mathbf{v}}_r\right)\mathrm{d}S = 0, \qquad (21)$$

in which $\bar{\mathbf{B}} = \partial\mathbf{N}'/\partial x$. The arbitrariness of the test function w implies that Eq. (21) should be fulfilled for any test vector $\mathbf{w}_e$, which leads to the following governing equation

$$\mathbf{S}\dot{\mathbf{p}}_e - \mathbf{C}'\dot{\mathbf{U}}_e + \mathbf{H}\mathbf{p}_e = \mathbf{Q}_e, \qquad (22)$$

where the matrices are defined as follows

$$\mathbf{S} = \int_L \mathbf{N}'^T\frac{\delta'_n}{K_w}\mathbf{N}'\mathrm{d}x,$$
$$\mathbf{C}' = \int_L \mathbf{N}'^T\mathbf{m}^T\mathbf{B}'\mathrm{d}x,$$
$$\mathbf{H} = \int_L \bar{\mathbf{B}}^T k'_t\delta'_n\bar{\mathbf{B}}\mathrm{d}x, \qquad (23)$$
$$\mathbf{Q}_e = \int_L \bar{\mathbf{B}}^T k'_t\delta'_n\rho_w g_t\mathrm{d}x - \int_S \mathbf{N}'^T\mathbf{n} \cdot \hat{\mathbf{v}}_r\mathrm{d}S.$$

Equation (22) and the related matrices in Eq. (23) are again of the same form as those of a solid element [19] except that most of the integrations in Eq. (23) are carried out along the long axis of the interface element.

For the implementation of a nonlinear coupling analysis, Eq. (22) is always written in an incremental form. To this end, the following assumptions within a time increment Δt are adopted

$$\dot{\mathbf{p}}_{t+\theta\Delta t} = \frac{\Delta\mathbf{p}}{\Delta t}, \quad \dot{\mathbf{U}}_{t+\theta\Delta t} = \frac{\Delta\mathbf{U}}{\Delta t}, \quad \mathbf{p}_{t+\theta\Delta t} = \mathbf{p}_t + \theta\Delta\mathbf{p}, \qquad (24)$$

where the subscript "e" is omitted for simplicity. The use of the mass balance equation at the instant $t + \theta\Delta t$ gives the following equation

$$\mathbf{C}'^T_{t+\theta\Delta t}\Delta\mathbf{U} - (\mathbf{S}_{t+\theta\Delta t} + \theta\Delta t\mathbf{H}_{t+\theta\Delta t})\Delta\mathbf{p}$$
$$= (\mathbf{H}_{t+\theta\Delta t}\mathbf{p}_t - \mathbf{Q}_{t+\theta\Delta t})\Delta t, \qquad (25)$$

which can be combined with Eq. (12) to give a more compact equation, i.e.

$$\begin{bmatrix} \mathbf{K}_{t+\theta\Delta t} & \mathbf{C}_{t+\theta\Delta t} \\ \mathbf{C}'_{t+\theta\Delta t} & -(\mathbf{S}_{t+\theta\Delta t} + \theta\Delta t\mathbf{H}_{t+\theta\Delta t}) \end{bmatrix}\begin{pmatrix} \Delta\mathbf{U} \\ \Delta\mathbf{p} \end{pmatrix} = \begin{pmatrix} \Delta\mathbf{F} \\ \Delta\mathbf{Q} \end{pmatrix}. \qquad (26)$$

For the sake of numerical stability, the interpolation factor θ in Eqs. (24)–(26) is often chosen to be greater than 0.5, i.e. $0.5 \leq \theta \leq 1.0$ [4]. Equation (26) gives the generalized stiffness matrix and the extended equivalent nodal force of the interface element, in which the incremental force vector $\Delta\mathbf{F}$ can be calculated according to the loading process and the incremental fluid flux vector $\Delta\mathbf{Q}$ evaluated via the right hand side of Eq. (25). Comparison of the coupling matrices $\mathbf{C}$ and $\mathbf{C}'$ given in Eqs. (13) and (23) shows that the generalized stiffness matrix of the interface element is symmetrical provided a symmetrical mechanical stiffness matrix. This is quite a favorable feature for numerical efficiency.

4 Numerical examples

In this section, the proposed interface element model is embedded into a finite element program FECAMM (finite element coupling analysis for multiphase media), and three examples are numerically solved for the verification of the model and the relevant formulations.

4.1 Hertzian contact problem

The Hertzian smooth contact problem is first investigated to check the validity of the mechanical contact model and the finite element code. An infinite cylinder with a radius of 1.0 m is vertically compressed by a load $F = 50\,\mathrm{MN/m}$ along the generatrix. Both the infinite foundation and the cylinder are assumed to be isotropically elastic and have the same parameters (Fig. 5a).

Hertz derived the analytical solution of this problem and found that the contact pressure along the contacting surfaces follows an elliptical distribution, where the maximum contact pressure q_0 and the contact width B read [10]

$$B = \sqrt{4F(k_1 + k_2)r}, \quad k_i = \frac{1 - \nu_i^2}{\pi E_i}, \quad q_0 = 2F/\pi B. \qquad (27)$$

Due to the symmetry of the model, half of the foundation and a quarter of the cylinder are discretized with 800 and 391 quadrilateral elements, respectively. Figure 5b shows a refined mesh near the contact surfaces. The probable contact surfaces are represented by 9 interface elements in accord with the solid mesh. This problem is solved numerically with the following parameters

$$\delta_{no} = 0.5\,\text{mm}, \quad h_s = 3\,\text{GPa}, \quad n = 0.5, \quad \mu = 0.0$$

all of which are empirically evaluated here without recourse to experiments. The translation of the geometrical nonlinear problem to an "equivalent" material nonlinear one results in a good performance in convergency and it can be expected that the numerical efficiency will be more evident for those elastoplastic contact problems, since only a layer of iteration for material nonlinearity is needed.

The numerical results predicted by the program FE-CAMM are compared with the analytical solution in Fig. 5c. Both the contact width B and the contact pressures at Gaussian integration points (the black dots) closely approximate the analytical solutions. The slight discrepancy of the contact pressure is mainly caused by the discretization of the contact surfaces, which can be effectively eliminated by using more interface elements with a higher order. The resolution of numerical solutions can be further improved by employing an adaptive FEM technique [20, 21], which, however, is beyond the scope of this paper.
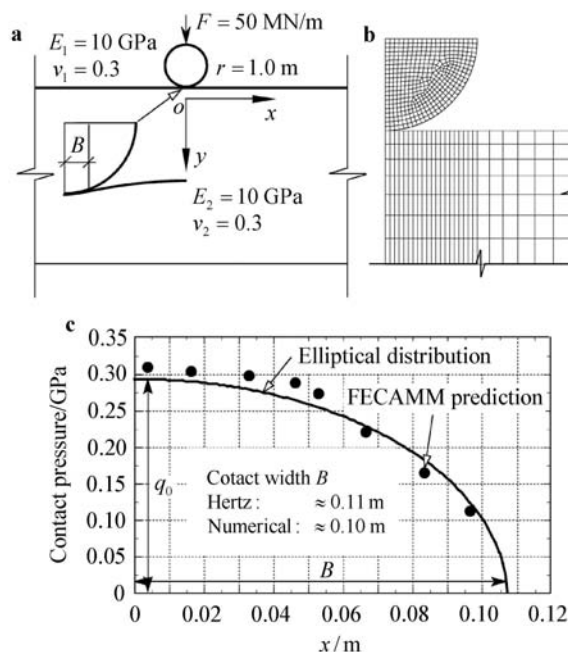
Fig. 5 Hertzian contact problem and its solution

Another source for deviation between the numerical and analytical solutions can be attributed to the difference that the non-penetration condition is satisfied approximately in the numerical model while the analytical solution is de-

rived without permission of penetration. Nevertheless, for most geotechnical applications, the precision of the numerical results seems to be acceptable.

4.2 Fracture seepage problem

To verify the fracture seepage model and the relevant formulations, the academic example devised by Segura and Carol [12] is studied. The problem consists of a gravity dam laying on a discontinuous medium, with the geometry and boundary conditions specified in Fig. 6. The permeability of the medium is assumed to be isotropic, with a seepage coefficient of $0.1\,\mu\text{m/s}$.
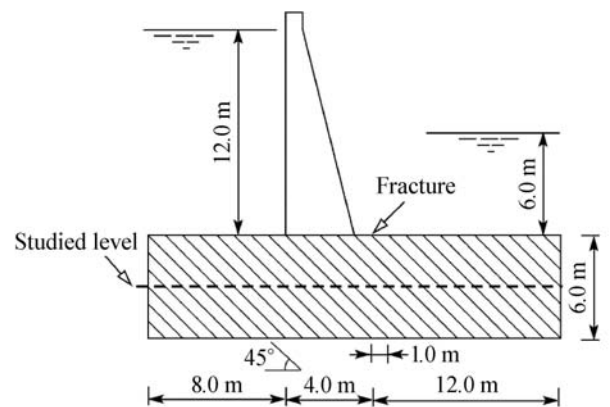
Fig. 6 Geometry of the fracture seepage problem

In this example, the deformation of the gravity dam and the base medium is neglected, and the interface between them is assumed to be impermeable. Only the steady-state seepage behaviour within the highly fractured medium is analyzed and the gravity of water is also neglected. The seepage domain is discretized with 318 quadrilateral solid elements and 288 interface elements.

In accordance with Segura's work, three different widths for the fractures are considered, i.e. $\delta'_n = 0.01$ mm, 0.05 mm and 0.1 mm, which according to Eq. (5) give the following values for the tangential seepage coefficient $k_t = 8.09 \times 10^{-5}$ m/s, 2.02×10^{-3} m/s and 8.09×10^{-3} m/s. Figure 7 gives the distributions of the hydraulic head at the level of 3 m below the ground surface predicted by FECAMM. For all the three cases, the hydraulic head at the investigated level decreases from the upstream to the downstream and the rate of decreasing is lower within both sides of the gravity dam than that underneath the gravity dam. The results provided by Segura and Carol [12] using their hydraulic interface elements are also plotted in Fig. 7 for comparison. It can be seen that the numerical predictions made by FECAMM are very close to the results of Segura in all three cases. This seems to indicate that the neglect of the transversal flow in our model does not result in an evident change of the hydraulic behaviour within the interface.

Comparing the three distributions shown in Fig. 7, we can also find that a slight change of the width of the fractures results in a considerable change of the hydraulic head in the base medium. These results confirm the necessity of taking the mechanical-hydraulic coupling effect along the interfaces into consideration in practical engineering. Only if the opening and the closure of the fractures are estimated reasonably, can the hydraulic responses within both the fractures and the surrounding media be predicted more realistically.
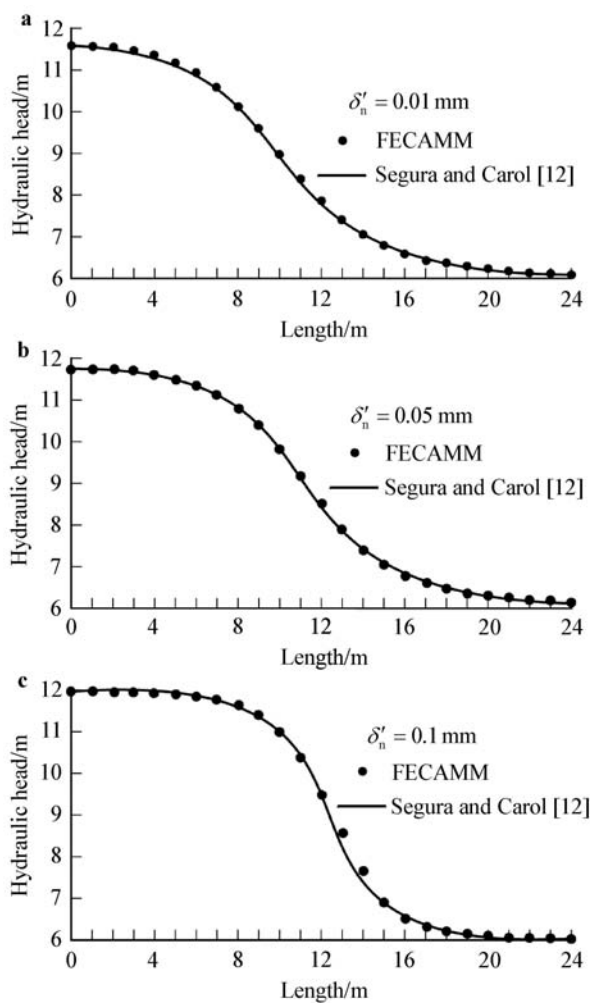
Fig. 7 The numerical solutions of the fracture seepage problem

4.3 Hydromechanical interface problem

The previous two examples check the mechanical and hydraulic performance of the interface element separately. The performance in coupling problems will be verified by this example. Two blocks of isotropically elastic material are separated by an interfacial gap which is fully filled with water as shown in Fig. 8. A uniformly distributed load is then exerted on the left surface of the left block, and the deformation of the two blocks is to be determined. Herein, the solid

blocks are assumed impermeable and two cases with different boundary conditions are investigated, i.e. the top of the interface is sealed and unsealed.
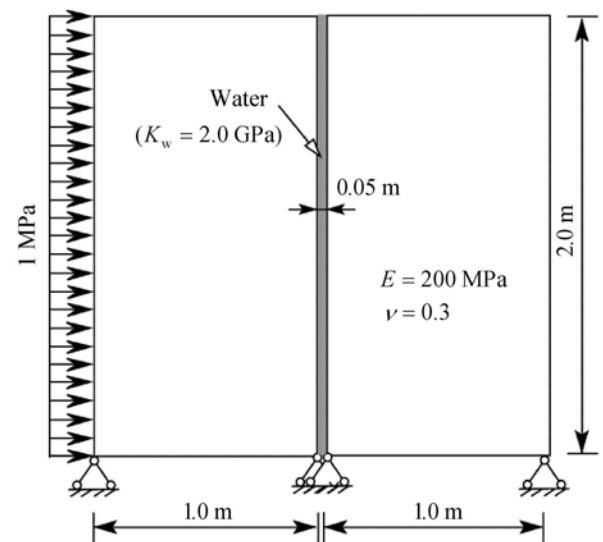
Fig. 8 Definition of the hydromechanical interface problem

The two solid blocks and the probable contact surfaces are discretized with 100 solid elements and 10 interface elements as shown in Fig. 9. The absence and existence of a top seal can be easily simulated by deactivating or activating the degrees of freedom for the pore pressure along the interface. In the absence of the seal, it is easy to infer that the left block will deform towards the right block and a certain portion of the interfacing surfaces will come into contact as shown in Fig. 9a. However, the presence of the top seal and the encapsulated water prevents such a deformation mechanism. The deformation of the left block will first result in a compression of the encapsulated water, which is bound to generate a fluid pressure (the magnitude of the fluid pressure is 483.5 kPa). The fluid pressure then identically acts on the interfacing surfaces and subsequently leads to a deformation of the right block. The deformed mesh in this case is also plotted in Fig. 9b. Qualitatively, the deformation modes depicted in Fig. 9 show a good coincidence with the conceptual analysis, and this confirms the reliability of the hydromechanical interface element and the relevant formulations derived in this paper.

5 Summaries and conclusions

The tribological interaction of two interfacing surfaces may result in deformation or breakage of the asperities built on the surfaces, leading to an apparent penetration. This physical consideration confirms the use of an interface element for the hydromechanical contact problem in this paper. The use of an interface element also makes the hydromechanical coupling effect along the interfacing surfaces easy to be con-
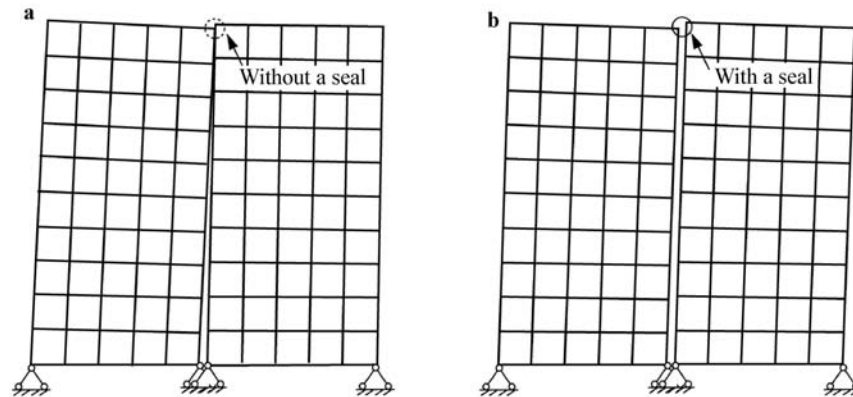
Fig. 9 The deformation modes of the hydromechanical interface problem

sidered, both when the surfaces are in or out of contact. This is benefited from the introduction of the effective thickness of the conducting channel for water, which is defined as the unachieved penetration, i.e. the maximal possible penetration in excess of the current penetration or interfacial gap.

The finite element formulations of the hydromechanical interface element were derived using the equilibrium equation of the interface and the mass conservation equation of the water within the effective conducting channel. The use of Terzaghi's effective stress principle and the consideration of the coupling effect along the solid- fluid interface make the governing equations fully coupled. Most of the involved matrices are of the same form as those of a solid element and can be assembled to the global stiffness matrix and the equivalent nodal force vector by the standard assembling procedure.

The proposed hydromechanical interface element was then incorporated into a finite element program and three simple examples were studied to check the validity of the model and formulations. Reasonable results confirm the feasibility of using the hydromechanical interface elements for coupled contact problems in geotechnical engineering.

References

1 Goodman, R.E., Taylor, R.L., Brekke, T.L.: A model for the mechanics of jointed rock. J. Soil Mech. Found. Div., ASCE **94**(3), 637–659 (1968)

2 Desai, C.S., Zamman, M.M., Lightner, J.G., et al.: Thin-layer element for interfaces and joints. Int. J. Numer. Anal. Meth. Geomech. **8**(1), 19–43 (1984)

3 Zhang, Y.T.: Rock Hydraulics and Engineering. China Water Power Press, Beijing (2005)

4 Rutqvist, J., Stephansson, O.: The role of hydromechanical coupling in fractured rock engineering. Hydrog. J. **11**(1), 7–40 (2003)

5 Liu, J.X.: A porosity-based model for coupled thermal-hydraulic-mechanical processes. [Ph.D. Thesis], The University of Western Australia, Perth (2009)

6 Guvanasen, V.: FRAC3DVS-OPG enhancement: subgridding, hydromechanical deformation and anisotropic molecular diffusion. Scientific Report (NWMO TR-2007-05), HydroGeoLogic, Inc. (2007)

7 Wriggers P.: Computational contact mechanics. John Wiley & Sons, Chichester (2002)

8 Zhang, H.W., Zhong, W.X., Gu, Y.X.: A combined parametric quadratic programming and iteration method for 3-D elastic-plastic frictional contact problem analysis. Comput. Methods Appl. Mech. Engrg. **155**(3-4), 307–324 (1998)

9 Zhang, H.W., He, S.Y., Li, X.S., et al.: A new algorithm for numerical solution of 3D elastoplastic contact problems with orthotropic friction law. Comp. Mech. **34**(1), 1–14 (2004)

10 Fischer-Cripps, A.C.: Introduction to Contact Mechanics. (2nd edn.) Springer, New York (2007)

11 Zhou, W., Zhou, C.B., Chang, X.L.: A contact model based on the SQP algorithm and engineering application. Appl. Math. Comput. **198**(2), 916–924 (2008)

12 Segura, J.M., Carol, I.: On zero-thickness interface elements for diffusion problems. Int. J. Numer. Anal. Meth. Geomech. **28**(9), 947–962 (2004)

13 Segura, J.M., Carol, I.: Coupled HM analysis using zero-thickness interface elements with double nodes. Part I: Theoretical model. Int. J. Numer. Anal. Meth. Geomech. **32**(18), 2083–2101 (2008)

14 Snow, D.T.: A parallel plate model of fractured permeable media. [Ph.D. Thesis], University of California, Berkeley (1965)

15 Tsang, Y.W., Tsang, C.F.: Channel model of flow through fractured media. Water Resour. Res. **23**(3), 467–479 (1987)

16 Simons, J.W., Bergan, P.G.: A finite element formulation of three-dimensional contact problems with slip and friction. Comp. Mech. **1**(2), 153–164 (1986)

17 Jing, L., Hudson, J.A.: Numerical methods in rock mechanics. Int. J. Rock Mech. Min. Sci. **39**(4), 409–427 (2002)

18 Berkowitz, B., Bear, J., Braester, C.: Continuum models for contaminant transport in fractured porous formations. Water Resour. Res. **24**(8), 1225–1236 (1988)

19 Lewis, R.W., Schrefler, B.A.: The Finite Element Method in the Deformation and Consolidation of Porous Media. John Wiley & Sons, New York (2000)

20 Wriggers, P.: Finite element algorithms for contact problems. Arch. Comput. Meth. Eng. **2**(4), 1–49 (1995)

21 Zienkiewicz, O.C., Taylor, R.L.: The Finite Element Method. Vol. 1: the basis. 5th edn. Butterworth-Heinemann, Oxford (2000)